

Design of Micropropulsion Plume Experiments

A Major Qualifying Project Report

Submitted to the Faculty

of the

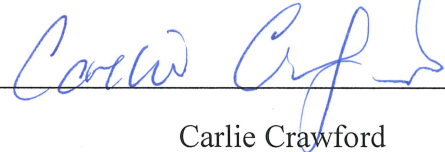
WORCESTER POLYTECHNIC INSTITUTE

in partial fulfillment of the requirements for the

Degree of Bachelor of Science

in Aerospace Engineering

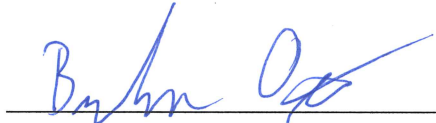
by



Carlie Crawford



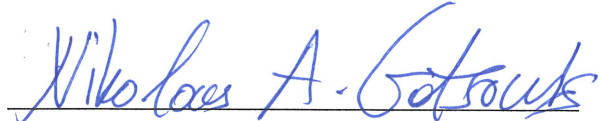
Jonathan Rodgers



Brandon Otte

February 27, 2013

Approved by:



Professor Nikolaos A. Gatsonis, Advisor

Aerospace Engineering Program

Mechanical Engineering Department, WPI

Abstract

This project involves design, analysis, and fabrication of a mounting assembly to be used within the Small Vacuum Facility-2 (SFV-2). The bell jar of SFV-2 includes a three degree-of-freedom positioning system for micropropulsion plume experiments. The fabricated mounting assembly allows the attachment of plasma diagnostics to the positioning system. Vibration data were collected with and without the SVF-2's mechanical pump running using accelerometers placed on the positioning system. Analysis shows random vibrations with maximum amplitude of 8 micrometers. The position uncertainty of a Langmuir probe is obtained with SolidWorks vibration analysis using amplitude inputs from the experiments. Calibration of the mass-flow system for the SFV-2 ion plasma source is also presented.

Acknowledgements

We would like to express our sincerest gratitude for Professor Nikolaos Gatsonis for providing us with research opportunity and his essential support and input along the way. We would also like to thank Michael Morin, a graduate student at Worcester Polytechnic Institute, for assisting and helping guide us throughout the project. Without these two influential people this project would not have been conceivable.

We would also like to thank Worcester Polytechnic Institute and Professor Gatsonis for providing us with all the necessary means to fulfill this project. This includes the use of the small vacuum chamber facility most of this project focused on, the equipment used to run all necessary tests, the machine shop for manufacturing parts of the project, and most importantly the education needed to make this project a reality. WPI really lives up to its motto "Lehr und Kunst" or "Theory and Practice" as with this support we were given an opportunity to apply the knowledge we gained over these past four years in this fascinating experience and actually turn theory into practice.

Authorship

Chapter 1

- 1.1 Crawford
- 1.2 Otte
- 1.3 Rodgers
- 1.4 Crawford, Rodgers, Otte

Chapter 2

- 2.1 Otte
- 2.2 Crawford, Otte

Chapter 3

- 3.1 Crawford, Rodgers
- 3.2 Otte

Chapter 4

Otte

Chapter 5

- 5.1 Crawford
- 5.2 Rodgers

Table of Contents

Abstract	2
Acknowledgements.....	3
Authorship.....	4
List of Tables	8
1. Introduction.....	9
1.1 Overview of Spacecraft Micropropulsion.....	9
1.2 Overview of Diagnostics of Electric Propulsion.....	10
1.2.1 Review of Langmuir Probes.....	10
1.2.2 Review of Retarding Potential Analyzers	11
1.3 Review of the Small Vacuum Facility	12
1.4 Objectives.....	13
2. Mechanical Design and Fabrication of the Probe Mounting System	15
2.1 Design Requirements	15
2.2 Design Process	16
3. Vibration Experiments and Analysis	19
3.1.1 Experiment Procedure	19
3.1.4 Facilities	23
3.1.5 Experiment Results and Discussion	23

3.2 Computational Vibration Analysis.....	27
4. Calibration of Mass Flow System.....	31
4.1 Calibration of Mass Flow System Experiment	31
4.2 Calibration of Mass Flow System Calculations	34
5. Summary and Recommendations	37
5.1 Summary and Conclusion	37
5.2 Recommendations	38
6. References.....	39
7. Appendix.....	40
7.1 List of Laboratory Materials	40
7.2 Data from Mass Flow System Calibration Experiment	42

List of Figures

Figure 1: TLP components and basic bias circuit schematic (Partridge, 2008).....	11
Figure 2: Schematic of the classical RPA electrode series (Partridge & Gatsonis, 2003).11	
Figure 3: SVF-2 in HL314 at WPI.....	13
Figure 4: Diagram of probe mount placement in SFV-2.	15
Figure 5: Second probe mount design.	17
Figure 6: Final probe mount design.	18
Figure 7: Vacuum pump located below table in SVF-2.	19
Figure 8: Dual mode vibration amplifier and oscilloscope setup.	20
Figure 9: Accelerometer calibration using hand-held shaker.	21
Figure 10: Positions of the accelerometer during vibration experiments.	22
Figure 11: One second vibration analysis graph without pump running.....	24
Figure 12: One second vibration analysis graph with pump running.	25
Figure 13: One second vibration analysis graph with pump running.	25
Figure 14: One second vibration analysis graph with pump running.	25
Figure 15: One hundredth of a second vibration analysis graph without pump running..	26
Figure 16: One hundredth of a second vibration analysis graph with pump running.....	26
Figure 17: One hundredth of a second vibration analysis graph with pump running.....	26
Figure 18: One hundredth of a second vibration analysis graph with pump running.....	27
Figure 19: SolidWorks TLP model.....	28
Figure 20: Results from vibrational analysis.	29
Figure 21: Mass flow system calibration setup.....	32
Figure 22: Bubble-O-Meter up close.	32
Figure 23: Barometer used for mass flow calibration experiment.....	35

Figure 24: Graph of volumetric flow rate vs. voltage for mass flow calibration..... 36

List of Tables

Table 1: STP volumetric flow rate at set voltages. 36

1. Introduction

Electric micropropulsion is used onboard spacecraft for attitude control, repositioning, and orbit changes (Ketsdever et al., 2000; Simon et al., 2006). Micropropulsion is any small scale propulsion device that generates a thrust in the order of micronewtons to a few millinewtons. The goal of our MQP is to develop and implement setups used in electric micropropulsion plume experiments. The setup includes a diagnostics positioning system to be integrated in WPI's Small Vacuum Facility-2 under integration in HL314.

1.1 Overview of Spacecraft Micropropulsion

Onboard micropropulsion is used to generate thrust. We are interested in electric micropropulsion which provides thrust through acceleration of ionized gases (or plasma) through electromagnetic fields. These plasma particles are created by the ionization of a propellant gas. Most commonly used as propellants are heavy inert gases such as xenon. However, there has been research done to use mercury or cesium as a propellant. A benefit of use electric micropropulsion is it reduces the total amount of propellant needed, resulting in a lighter satellite.

There are several types of electric micropropulsion thrusters that fall under electrothermal, electrostatic, and electromagnetic categories. Electrothermal thrusters include the resistojet and the arcjet. This propulsion process is when a propellant is heated in a chamber and expanded creating the thrust necessary. Electrothermal thrusters have specific impulse, I_{sp} , defined as the ratio of exhaust velocity to gravitational acceleration, in the range of 300-600 seconds. Electrostatic propulsion includes primarily ion thrusters. These thrusters utilize plasma technology to ionize the propellant being used allowing it to be accelerated through grids via electrostatic forces. Ion thrusters have an I_{sp} in the range for 2500-3600 seconds and efficiency

of about 60-80%. Finally, electromagnetic propulsion devices include the pulsed plasma thrusters (or PPT). These thrusters ablate and ionize a solid propellant, usually Teflon, into a plasma arc and accelerate the plasma by electromagnetic forces delivering an Isp in the range of 800-1200 with efficiencies of about 7-13% (Goebel and Katz, 2008).

1.2 Overview of Diagnostics of Electric Propulsion

Investigation of electric micropropulsion involves measuring properties of the plasma plume, including the electron number density, electron temperature, plasma space potential, ion drift velocity, and constituent species concentration. These measurements provide the understanding of acceleration mechanisms in the thruster and also allow evaluation of potential impacts on spacecraft. Plasma plume diagnostics include Langmuir probes, triple Langmuir probes, Quadruple Langmuir Probe (QLP) and Retarding Potential Analyzer (RPA). (Partridge 2008) We review below some of these diagnostics.

1.2.1 Review of Langmuir Probes

Langmuir probes are biased wires immersed into plasma. Measuring the collected current as a function of applied potential allows for the determination of the electron density, electron temperature, and electron potential. Different types of Langmuir probes exist, consisting of Single Langmuir Probes (SLP), Double Langmuir Probes (DLP), Triple Langmuir Probes (TLP), and Quadruple Langmuir Probes (QLP). For this MQP the focus will be on the QLP (Partridge 2008). A QLP is much like the TLP but make use of a cross probe that is perpendicular to the plasma flow. The TLP is made up of three exposed conductive wires (commonly Tungsten) that run parallel to the mean plasma flow direction. Time-resolved measurements of the electron temperature, electron number density, and plasma space potential are calculated by using the relevant TLP current-mode theory of operation with the monitored current pulses between each

probe wire and the plasma. These pulses are monitored by the application of voltages between probe wires 1 and 2 and also wires 1 and 3. A schematic of a TLP and bias circuit is shown in Figure 1. The addition of a fourth probe wire that runs perpendicular to the plasma flow creates what is known as the QLP. Examining the current through the cross probe allows for the measurement of the ion speed ratio in addition to the measurements of the other probe wires (Gatsonis et al., 2004).

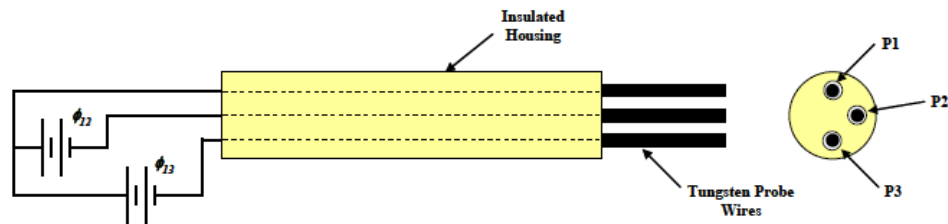


Figure 1: TLP components and basic bias circuit schematic (Partridge, 2008).

1.2.2 Review of Retarding Potential Analyzers

Another diagnostic of interest to this MQP is the Retarding Potential Analyzer (RPA). These employ a series of variable biased electrodes to filter incident plasma flux allowing only high energy ions and neutrals access to a collector plate. A schematic of the RPA electrode series is shown in Figure 2.

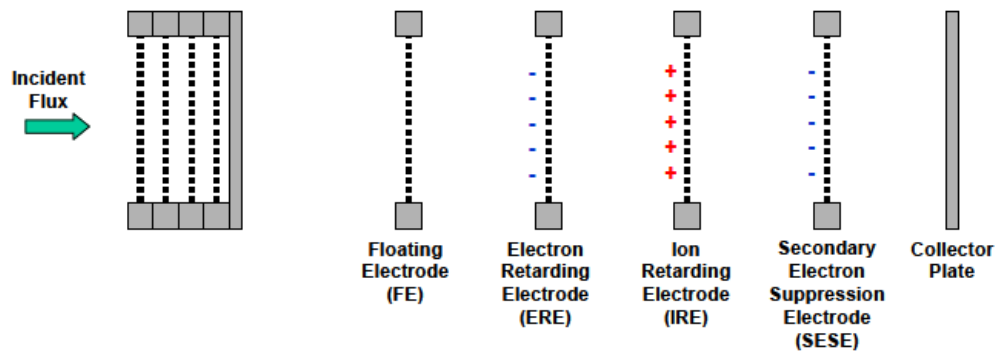


Figure 2: Schematic of the classical RPA electrode series (Partridge & Gatsonis, 2003).

The first electrode is known as the Floating Electrode, which provides incident plasma with a germane interface and allows the average plasma or space potential to be monitored. The second electrode is the Electron Retarding Electrode which is biased negatively so as to repel all incident electrons. The third electrode is the Ion Retarding Electrode which is biased positively to repel low energy ions. The bias is varied throughout an experiment from zero up to the limit where all ions are repelled away. This produces an I-V curve which can be analyzed to determine several plume properties such as ion number density, ion temperature, ion drift velocity, and constituent species concentrations. The last electrode is a Secondary Electron Suppression Electrode biased negatively to repel any secondary electrons which may have been emitted throughout the electrode series. These electrodes are separated by an insulating material like Teflon or nylon. Finally the collector plate current is closely monitored at various ion retarding potential settings to populate the I-V curve. (Partridge, 2008)

1.3 Review of the Small Vacuum Facility

Plume investigations of electric propulsion thrusters are taken place in vacuum chambers. The Small Vacuum Facility-2 (SVF-2) in HL314, shown in Figure 3, is composed of a table, a 0.20839 m^3 (12717 in^2) stainless steel bell jar (0.28575 m (11.25 in) radius and 0.8128 m (32 in) height) and associated electronics the cover of the bell jar that is lowered into position by a hydraulic pump to create a seal. The vacuum chamber requires delicate operation around it during use due to the fact that the bell top can be nudged and will prevent a good seal from occurring when it is lowered into position. In addition, the surface where the bell top touches the other half of the chamber must not be scratched so that there is a uniform seal. The chamber is pumped using a diffusion pump installed on the bottom of the vacuum chamber.



Figure 3: SVF-2 in HL314 at WPI

The SVF-2 was constructed in a series of MQPs [NAG-0902, NAG-1101] and work of Morin [2013]. In order to accommodate planned plume experiments the MQP NAG-1101 designed a setup to support both the micropropulsion thruster as well as the instrumentation required to make plume measurements shown in Figure 3. The setup allows for adjustable positioning of the diagnostic instrumentation across multiple locations of the vacuum chamber in order to make the necessary readings during experimentation. The goal of this MQP group is to complete the design and construction of the setup and integration of the SFV-2.

1.4 Objectives

The first objective is to design and fabricate a mounting system for the QLP and TLP to use in the SFV-2.

- Requirements: The design must accommodate the QLP, TLP and future diagnostics while also fitting within space limitations of the small chamber; holding the diagnostics in place without interfering with the motor.
- Approach and Methods: Given the dimensions, undergo multiple mount design iterations using SolidWorks and once finalize fabricate the mount.

The second objective is to analyze the effects of possible vibrations within the translation structure to determine any position error that could occur in the measurements of the plasma plume.

- Requirements: Assume that the vibrations during the worst case scenario are constant and find the effects that this worst case has on the displacement of the probes.
- Approach and Methods: Simplify the translation structure and create a TLP model in SolidWorks. Design an experiment utilizing accelerometers and measure the vibrations of the translation structure in the vacuum chamber. Use the data as inputs for the computational vibration analysis in SolidWorks.

The third objective involves the calibration of the mass flow system.

- Requirements: Calibrate the mass flow system used in plasma plume experiments.
- Approach and Methods: Run experiments to determine the mass flow rate of the system at various voltages and calibrate the mass flow system accordingly.

The fourth objective is to create a list of all the hardware used to run the SVF-2 and compile all of the necessary manuals. Then to make both a large binder copy of all the manuals and a digital folder version of all the .pdf versions of the manuals. This objective and process will not be covered later in the report but the SVF-2 manual can be found in HL314.

2. Mechanical Design and Fabrication of the Probe Mounting System

One of the primary objectives of this MQP is the design and fabrication of a mount to hold the QLP and RPA in position during the plasma plume experiments. In this chapter the original requirements for the mount as well as the ideas used to fulfill these requirements are discussed. Also the original design plans and the process to reaching the final version and fabrication of the probe mount will be outlined.

2.1 Design Requirements

A number of requirements needed to be met in order to allow for the diagnostic devices to be properly mounted within the SFV-2. The design had to allow for the positioning of the diagnostic device or probe in such a way that the probe tip would be centered at the pitching point of the motor so that as the mount moved the tip of the probe would not change position. In addition the mount had to be flexible enough to allow for the interchange of different sized diagnostic devices with ease. The SolidWorks model of the translation structure with the old mount can be seen in Figure 4 the red arrow shows the position of the mount.

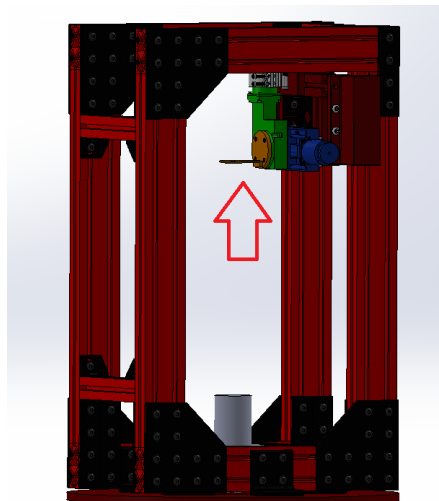


Figure 4: Diagram of probe mount placement in SFV-2.

2.2 Design Process

The first requirement to keep probe tip centered at the pitching point of the motor was accomplished by having a bar extend upward and then an L-bracket reached outward such that the probe would be above the thruster. The length of this bar is restricted to 17 cm so that as it is rotated no contact with any of the beams of the translation structure will occur. The length of the designed piece was kept to 16 cm thus restricting probe size to be smaller than 16 cm. In addition to contact with the beams, the bar would impact part of the motor without the use of a spacer, so a 1.27 cm (0.5 in) spacer is located in between the bar and the base of the mount.

In order to allow for different size probes a $\frac{1}{4}$ in threaded hole is located at the top of the mount on the L-bracket such that the probe can be screwed right into it. The probe will need a way of being screwed into this hole and it is highly recommended that the device include a Swagelok fitting. Swagelok has a variety of different size fittings and converters allowing for the use of devices of varying size to be easily interchanged while keeping the tip in the proper place. At first a circular bar with a female and male end was going to be used as an extender. The problem with this however was that a new extension would be needed for each probe being used. This lack of flexibility caused us to move in the direction of the mount depicted in Figure 5

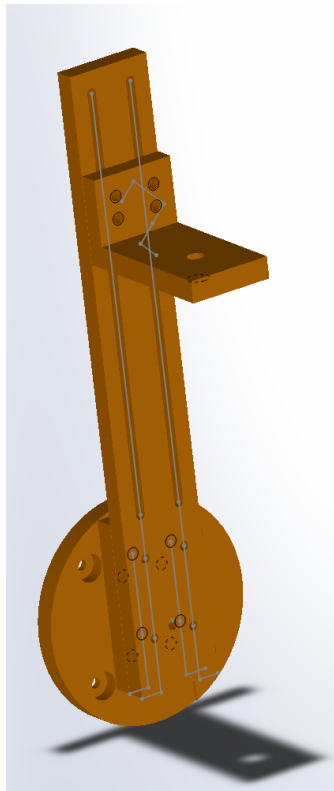


Figure 5: Second probe mount design.

The rail system seen by the two parallel slotted lines in Figure 5 was designed to better accommodate probes of different length to be mounted onto the system. Once mounted the rail would be adjusted to allow the tip of the probe to remain centered about the point of rotation of the mount during testing. The L-bracket that slides along the top of the rail is designed to create a larger base for the weight of the probe to be locked down and prevent drooping; once again maintaining the probe tip centered above the center of rotation.

However, once machining was started a couple flaws with this design became evident. Due to the size of the slits in the mount compared to the rest of the material the piece would buckle during machining and cause warping that would make any data measured inaccurate. The final design of the mount as seen in Figure 6 uses two brackets to work as a clamp when tightened firmly holding the L-bracket in place. At the base of the mount a hole just below the

center can be seen. A small threaded bar will be screwed into this to mark the center while mounting the probe allowing for accurate positioning. The mount system is made out of Aluminum, the same material used for the rest of the translation structure, due the material being vacuum compatible and is much easier to work with than stainless steel, in addition it is rather inexpensive.

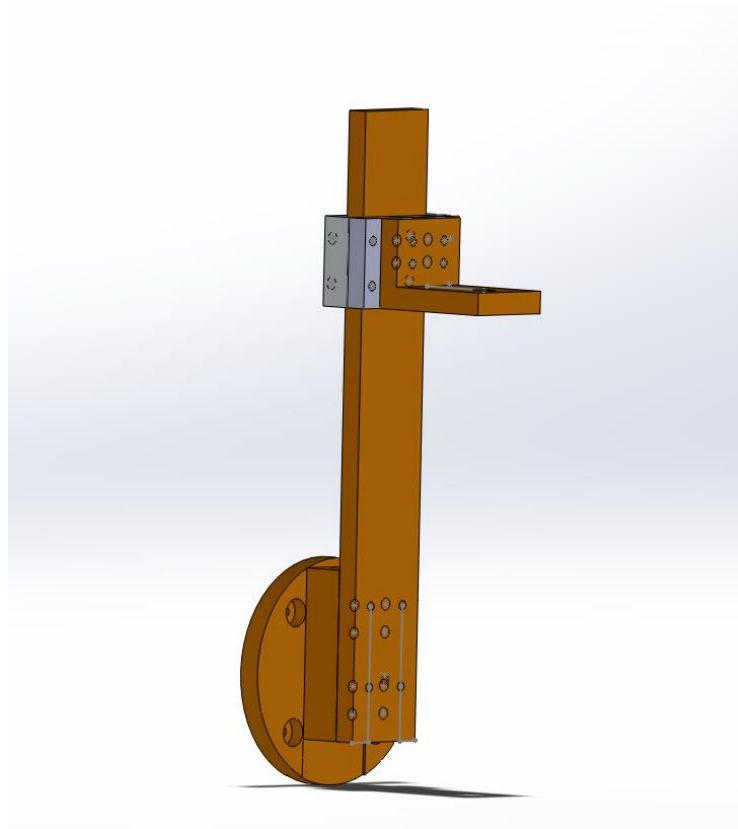


Figure 6: Final probe mount design.

3. Vibration Experiments and Analysis

In this chapter we describe experiments to determine the impact of the mechanical pump vibrations on the uncertainty in probe positioning using the probe mount discussed in Chapter 2. Using an accelerometer positioned along the X-Y-Z axis near the mount location, measurements were taken to estimate the displacements induced during pump operation of the SVF-2. Inputs were also used to run vibrational analysis in SolidWorks.

3.1.1 Experiment Procedure

The purpose of this experiment was to use accelerometers to measure vibrations induced on the diagnostics mount from the vacuum pump in SFV-2. The objective was to determine whether these vibrations would have any positioning error on the planned plume experiments.

The experiments took place in the Fluid and Plasma Dynamics Lab (FPDL) in HL314. The SVF-2 is located on top of a table with a hole cut through the bottom to allow a vacuum pump to vacate the air. The pump is then located on a truss below the table and proceeds to feed through aforementioned hole as shown in Figure 7.



Figure 7: Vacuum pump located below table in SVF-2.

After calibration using a hand-held shaker, a shear accelerometer was mounted directly on the table within the SFV-2 bell jar. It was then connected to the dual mode vibration amplifier (Model 443B01), which is used to amplify the voltage signal from the accelerometer and then integrate the acceleration to a position. The position signal is then sent from the dual mode amplifier to the oscilloscope where final calibrations are made before being sent to a computer. Before running the experiment, the dual mode amplifier had to be adjusted in order to properly read and convert the data collected. This was done by manually changing the input to correctly match the accelerometer used and the output to the desired amplification and integration. For this experiment the first accelerometer signal was amplified and integrated from $1.013 \frac{mV}{\frac{m}{s^2}}$ to $1000 \frac{mV}{mm}$ (or $1.0 \frac{mV}{um}$) and a second accelerometer signal of $10.13 \frac{mV}{\frac{m}{s^2}}$ was also converted to $1.0 \frac{mV}{um}$ to additionally verify the results. The setup of the dual mode vibration amplifier and oscilloscope can be seen in Figure 8.

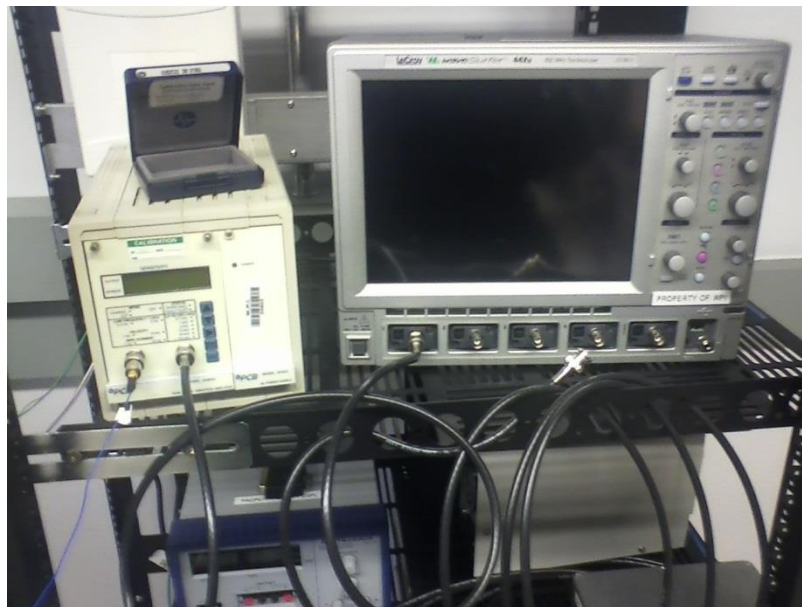


Figure 8: Dual mode vibration amplifier and oscilloscope setup.

The experiment was run a total of six times using two different accelerometers. First the accelerometers had to be calibrated using a Hand Held Shaker (Model # 394C06). The accelerometers were mounted to the top of the shaker (see Figure 9), and then once powered on the shaker then provides a vibration of $100 \frac{mV}{\frac{m}{s^2}}$. This is done to verify the output on the oscilloscope matches the constant vibration of $100 \frac{mV}{\frac{m}{s^2}}$ from the shaker. This ensures the whole system is calibrated properly outputting accurate results. A figure of the accelerometer calibration using the shaker is shown in Figure 9



Figure 9: Accelerometer calibration using hand-held shaker.

The first experiment was performed with the accelerometer that has a sensitivity of $1.013 \frac{mV}{\frac{m}{s^2}}$ located on the x-axis of the table, then on the y-axis, and followed by the z-axis. The positioning of the accelerometer for each run can be seen by the red dots in Figure 10 The experiment was repeated using an accelerometer with a sensitivity of $10.13 \frac{mV}{\frac{m}{s^2}}$. In order to keep

the accelerometers steady on the table the bottoms were coated in wax and then seated. For each run through the experiment began with the pump deactivated and after a baseline was established the pump was then turned on so further data could be record with it activated. These tests were not recorded because the oscilloscope that was being used did not have the parts needed to save the data and transfer it to a computer. However, data from the visual display of the Tektronix oscilloscope showed a range of about ± 10 micrometers.

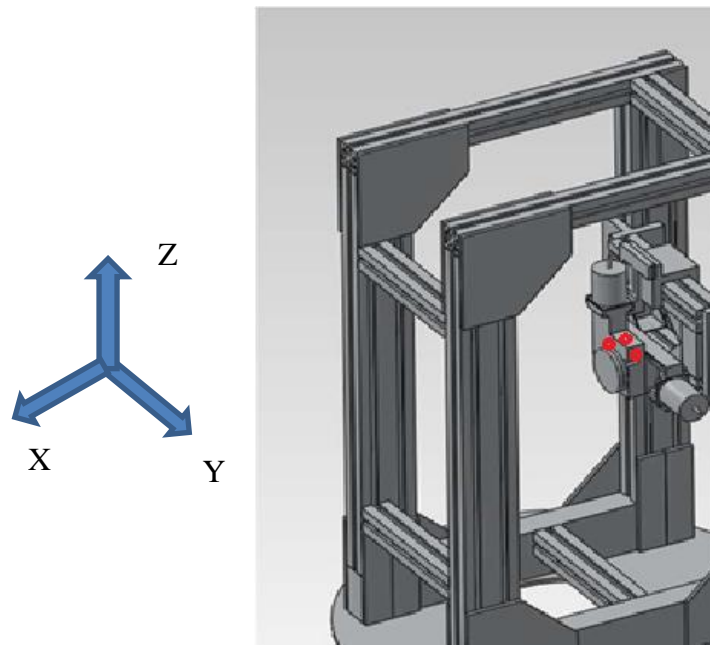


Figure 10: Positions of the accelerometer during vibration experiments.

Complete measurements with the LeCroy Oscilloscope were taken and the recorded displacement data were entered into an excel spreadsheet. For this experiment, the framework for the probe was assembled and placed inside the vacuum chamber and the accelerometer was placed as close to the location of the probe as possible. Four measurements were taken with the accelerometer. The first test was the vertical displacement while the pump was running. The second test was along the same axis but without the pump running in order to get a baseline. The

third and fourth tests measured horizontal movement along two perpendicular axis and these were with the pump running as well.

3.1.4 Facilities

- Dual Mode Vibration Amplifier Model 443B01
- Tektronix TDS2000-Series Digital Storage Oscilloscope
- LeCroy Wavesurfer 44Xs Oscilloscope
- Micropropulsion experimental vacuum chamber
- Shear Accelerometer Model # U352C22
- Shear Accelerometer Model # 352A24
- Wax
- Hand Held Shaker Model # 394C06

3.1.5 Experiment Results and Discussion

The first experiment, shown in Figure 11, shows the vertical displacement while the pump was running. The second experiment, as shown in Figure 12 was along the same axis but without the pump running in order to get a baseline. The third and fourth tests measured horizontal movement along two perpendicular axis and these were with the pump running as well (see Figures 13 and 14).

Although this experiment was carried out with every precaution in order to ensure that accurate data was obtained, it is likely that experimental errors are present. One possible source of error could be due to the noise level. There was an unaccounted noise level in the vibration analysis that prevented measurements being taken within ± 8 micrometers. This could either be because of a minor fault in the equipment or an ambient vibration from something other than the mechanical pump causing a vibration in the table. In order to improve the experiment, a damper

could be mounted to the table and eliminate background vibrations. This would potentially remove the noise and ensure the vibrations recorded are solely due to the mechanical pump.

Another, explanation for the noise recorded is due to resolution of the system. While the devices were rated to measure on the micron level we believe that we had exceeded what they could practically record. Figures 15-28 show the displacement over a period of one-thousandths of a second, the vibration is very erratic. However, by creating a moving average line a sinusoidal wave begins to emerge. This is interesting because in Figure 12, which shows the full second of data, there is a similar occurrence. By taking a moving average line for those graphs another sinusoidal line appears. In Figure 12, it looks as though there are at least two waves creating constructive/destructive interference with one another. However, the frequencies for the waves in the short graphs are around 12500 Hz while the longer graphs are around 15 Hz. The difference between these two causes our team to believe that the vibrations detected from the graphs only looking at one-one thousandths of a second to be noise and that the waves from the graphs looking over a longer period of time to contain the actual vibrations we are looking for.

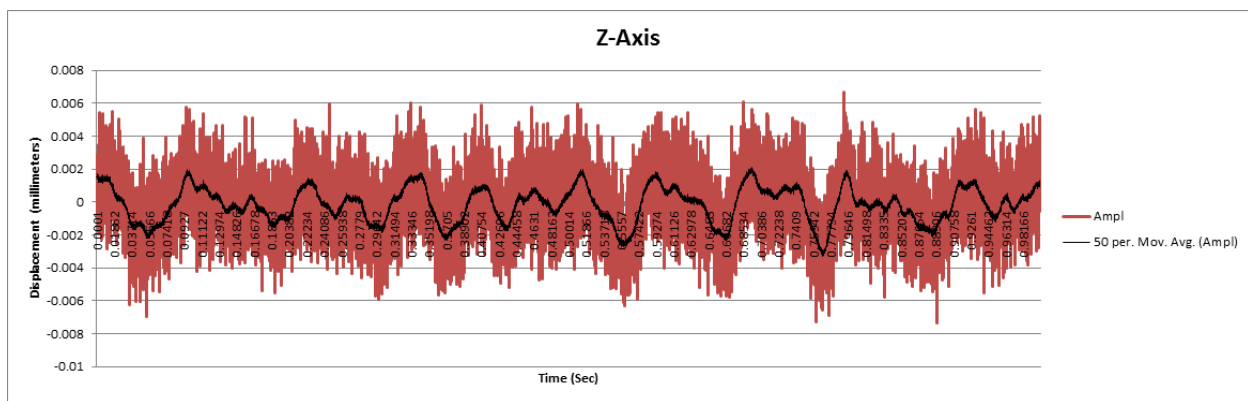


Figure 11: One second vibration analysis graph without pump running.

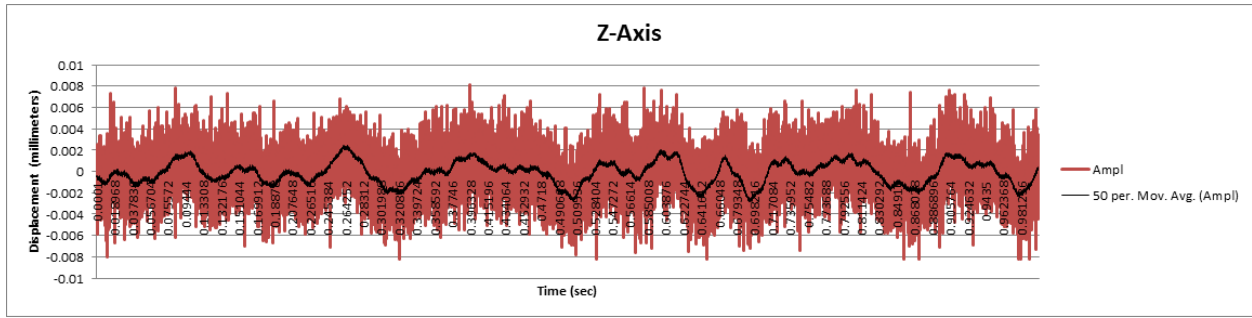


Figure 12: One second vibration analysis graph with pump running.

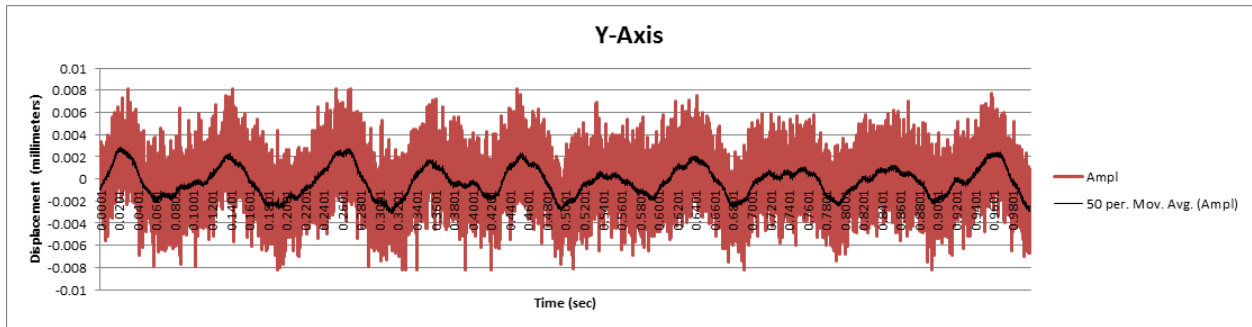


Figure 13: One second vibration analysis graph with pump running.

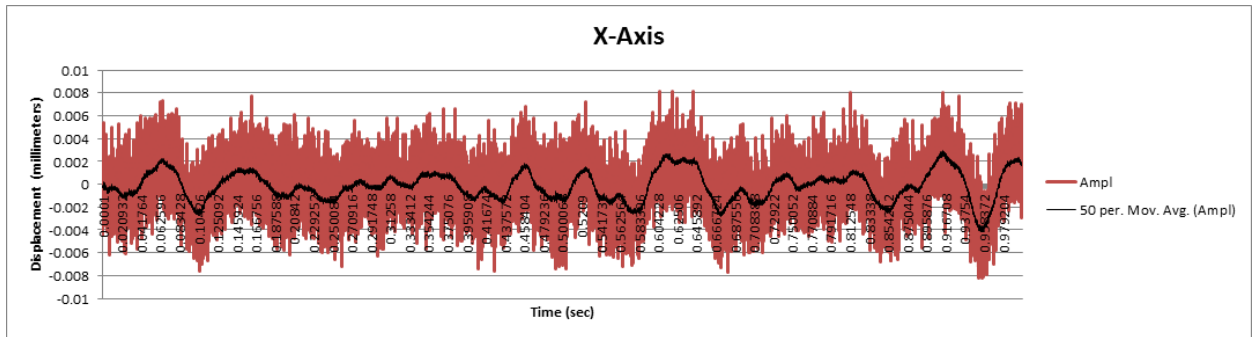


Figure 14: One second vibration analysis graph with pump running.

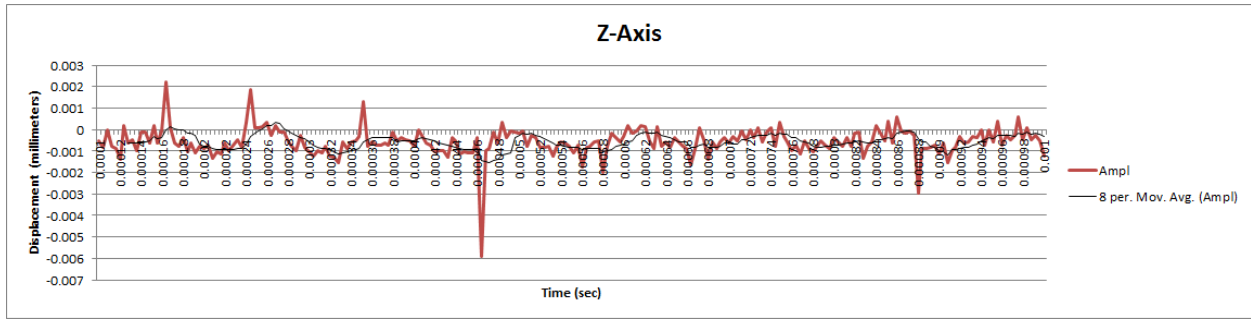


Figure 15: One hundredth of a second vibration analysis graph without pump running.

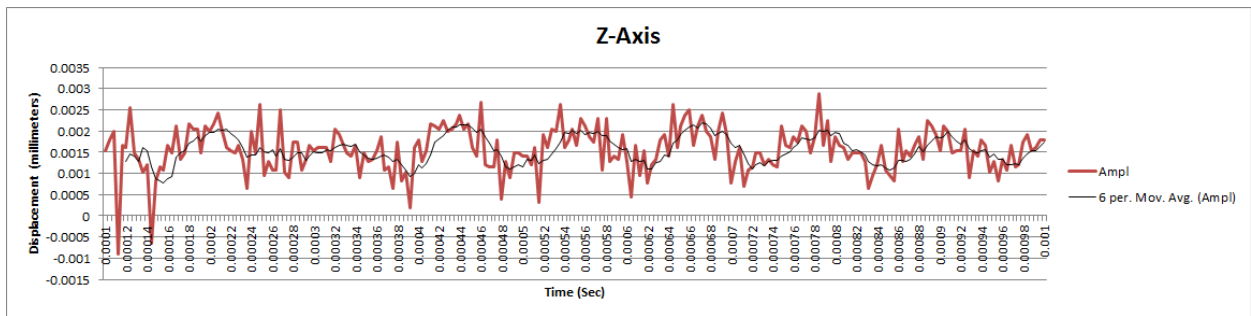


Figure 16: One hundredth of a second vibration analysis graph with pump running.

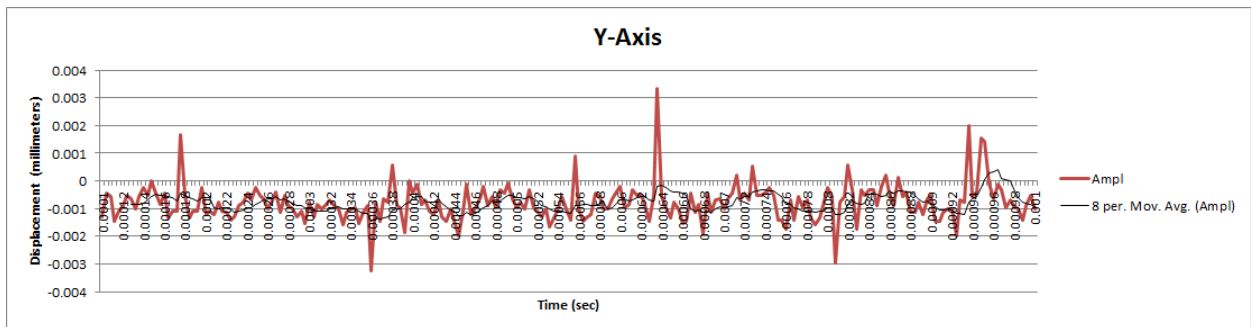


Figure 17: One hundredth of a second vibration analysis graph with pump running.

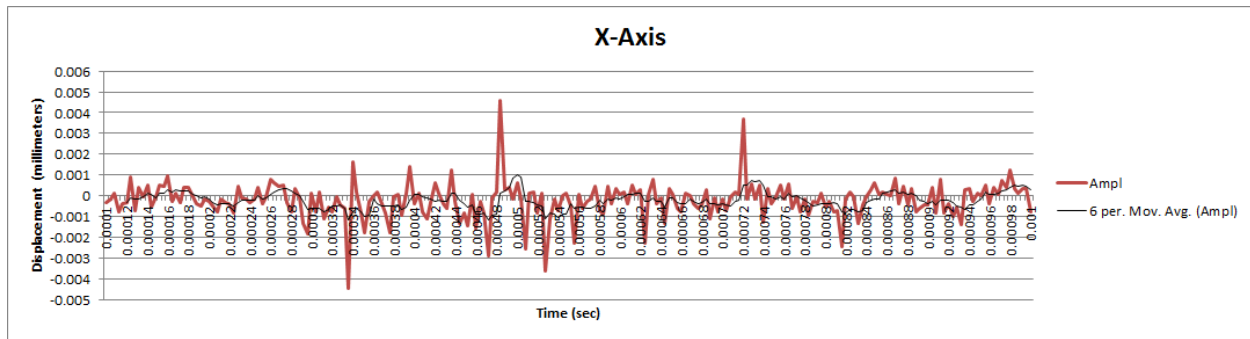


Figure 18: One hundredth of a second vibration analysis graph with pump running.

3.2 Computational Vibration Analysis

During pump operation, small vibrations throughout the entire system occurred. These vibrations cause uncertainty in the position of diagnostics measurements and need to be accounted for. In order to assess the impact of these vibrations, the entire translation structure was decided to be imported into COMSOL for analysis. Due to computational limitations meshing of the translational structure is not possible and thus it was necessary for the structure to be simplified (de-featured). However due to the fact that the displacement data from the actual experiment came from the accelerometer being placed directly onto the structure instead of on the table as previously planned, the simplification did not end up being needed.

Instead a TLP model was created in SolidWorks for the analysis and also allowed for vibration computations to be done directly in SolidWorks. The TLP model was created using the guide for making TLP and QLP's of Partridge [2008, Appendix]. The TLP consists of borosilicate glass tubing, tungsten wires, polysilica tubing as an insulator for the wires, (Partridge 2008) and aluminum ¼ in. Swagelok fitting for connecting to the mount (a simple cylinder is modeled to represent this). All of the materials for each part needed to be included to create accurate results. The model used for the vibrations is shown in Figure 19.

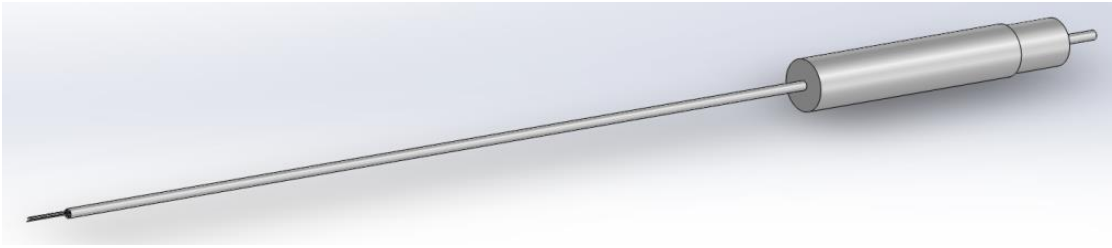


Figure 19: SolidWorks TLP model.

Proper meshing of the assembly within SolidWorks proved to be rather difficult in some areas of the model due to the small surfaces present and memory availability for resolution. However creating a curvature based mesh as opposed to the standard mesh and using meshing controls to increase the resolution in the smallest areas and leave the resolution low in others an acceptable mesh of the probe was created. For the simulation three selected base displacement excitations were applied at the top face of the modeled Swagelok fitting in the X-Y-Z directions. Two different vibrations were evaluated, first the vibrations caused by the average displacement value from the experiment of 2 micrometers and again for the maximum displacement of 8 micrometers. Both of these values were applied at a time sine wave from 0s to 1s with amplitude of 1 and a frequency of 75.4 rad/s. The frequency was estimated by counting the number of spikes from the graph produced during the experiment (12) and then multiplying by 2π . Running of the simulations produced the results in Figure 20.

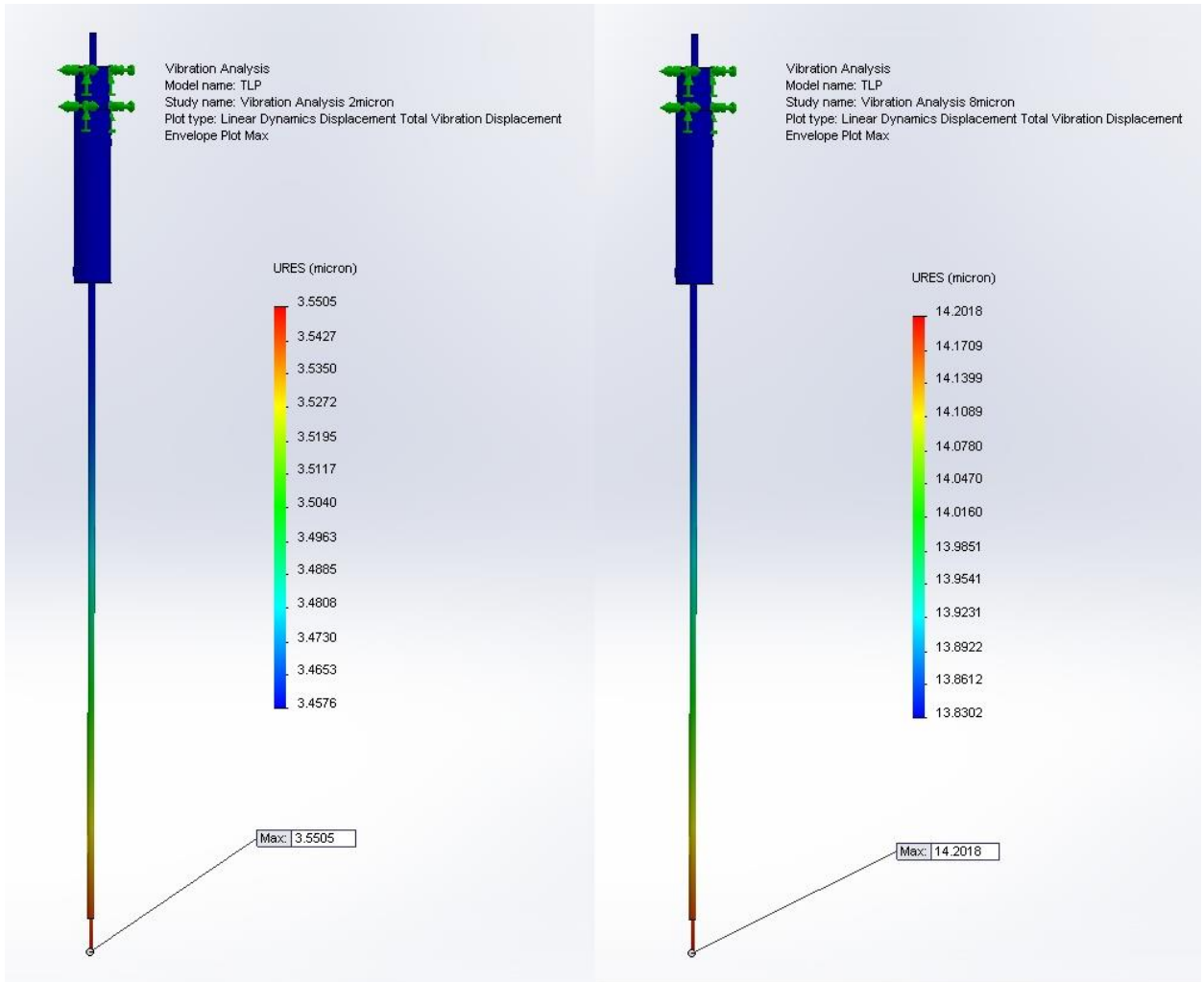


Figure 20: Results from vibrational analysis.

The base displacement excitations applied were in component form however the results from the simulation show the magnitude of these displacements at the face of the Swagelok fitting. The simulated vibrations permeating through the probe caused the magnitude of the maximum displacement to increase as observation moves further down the probe away from the Swagelok fitting, with the maximum displacement occurring at the probe tip. The additional displacement at the tip of the probe due to the vibrations during the 2 micrometer and 8 micrometer simulations totaled 0.0929 micrometers and 0.3716 respectively. It can also be noted that the vibrational displacement is directly proportional to the initially applied displacement.

This extra displacement caused by these vibrations may cause minor error in future experiments however the error due to human positioning of the probe is more likely to affect the data of the plasma micropropulsion plume experiments than the error due to the propagations of these vibrations.

4. Calibration of Mass Flow System

The main focus of the experiments in the SVF-2 is to measure the properties of a plasma plume produced by an ion source. The plasma source used in these experiments is a Kaufman ion source utilizing Argon as the propellant. The mass flow of argon to the ion source is controlled by the mass flow system. Apart from the ion source and the canister of Argon the mass flow system consists of a VWR regulator, MKS mass flow controllers, meter, and power supply, and Swagelok DI/DS Series Diaphragm Valves. More hardware information such as serial numbers is located in Appendix 7.1 and manuals are located in HL314. This system has never been calibrated and so the readout on the mass flow meter is inaccurate. In this chapter the calibration process for the mass flow system will be explained.

4.1 Calibration of Mass Flow System Experiment

To accurately control the mass flow of the argon to the Kaufman ion source a calibration process of the mass flow system is necessary. Without calibration actual mass flow of Argon will be different than the measured mass flow, causing the data throughout experiments to be fairly inaccurate. To calibrate the mass flow system a Bubble-O-Meter 1-10 ml soap bubble gas flow meter was used in addition to the bubble solution, a clamp test stand, syringe, stopwatch, thermometer, barometer, and a computer, connected to the mass flow controller, with a MATLAB program for sending and reading the voltages to the controller. The setup, excluding the barometer and computer, can be seen in Figure 21 and 22.



Figure 21: Mass flow system calibration setup.



Figure 22: Bubble-O-Meter up close.

The Bubble-O-Meter, held up by the clamp test stand, is connected at the bottom by a tube directly to the mass flow controller output, and filled with bubble solution; just enough so as when the stopper at the bottom is squeezed the solution will block the Argon gas flow causing a bubble to form and when released no longer will block the flow causing the bubble to slowly move up the Bubble-O-Meter. It is necessary to make sure that the Bubble-O-Meter is clean and the sides of the tube are sufficiently wet with the bubble solution as to allow the bubble formed to move up the tube undisturbed preventing it from popping. Using the MATLAB program on the computer to control the voltage output to the mass flow controller, the flow of Argon through the Bubble-O-Meter can be regulated. The desired voltage and actual voltage supplied to the mass flow controller are slightly different and so the actual voltage read is also measured through the MATLAB program during operation.

Setting a voltage to the mass flow controller of 0.5 V yielded an average actual voltage read of 0.4883 V. Using this voltage to control the mass flow of Argon a bubble was created and allowed to climb the inside of the Bubble-O-Meter. Also the barometer and thermometer were both closely monitored to record the pressure and temperature of the room. On the Bubble-O-Meter there are three lines, the first to mark the starting point, the second to mark 1ml, and the third to mark 10 ml. As the bubble crosses the starting point the timer on the stopwatch is activated to time the ascent of the bubble. If the bubble reaches the 1ml mark in fewer than 30s the data will not be accurate enough so the bubble is then allowed to ascend to the 10ml mark if not the timer on the stopwatch is stopped and the time recorded. The only voltage that the bubble took over 30 s to reach the 1 ml mark was 0.5 V, all other voltage settings the bubble was required to reach the 10 ml mark. This was repeated 7 times for the following voltages: 0.5 V, 1.5 V, 2.5 V, 3.5 V, 4.5 V, and 5 V. The recorded data from the experiment is located in Appendix 7.2.

4.2 Calibration of Mass Flow System Calculations

From the data gathered during the calibration experiment a number of calculations needed to be made to find the volumetric flow rate to calibrate the system. Using the time the bubble took to ascend the Bubble-O-Meter the volumetric flow rate can be calculated by dividing the volume by the time the bubble took to travel the volume.

$$Q = \frac{V}{t}$$

This mass flow rate however is only at the current temperature and pressure and does not take into account the effects of water vapor from the bubble. Due to this it is necessary to convert to standard temperature and pressure (STP) conditions, $T=273\text{K}$ and $P=100\text{kPa}$, and to remove the effect of the water vapor pressure. First the water vapor pressure must be calculated at each temperature using the Antoine equation where P is the vapor pressure, T is the temperature in $^{\circ}\text{C}$, and A , B , and C are the constants 8.10765, 1750.286, and 235 respectively. (Felder & Rousseau 2005)

$$\log_{10}(P) = A - \frac{B}{C + T}$$

The yielded water vapor pressures fell in the range of 2800-3000 Pa. These pressure values need to be subtracted from the pressure in the room, 101698 Pa (14.75 psi), while converting to STP. The original recording for the room pressure was 41.5 psi, however this impossible room pressure was due to the misreading of the barometer needle, which can rotate twice allowing for readings up to 50 psi. The actual pressure should be 14.75 psi as seen in Figure 23.

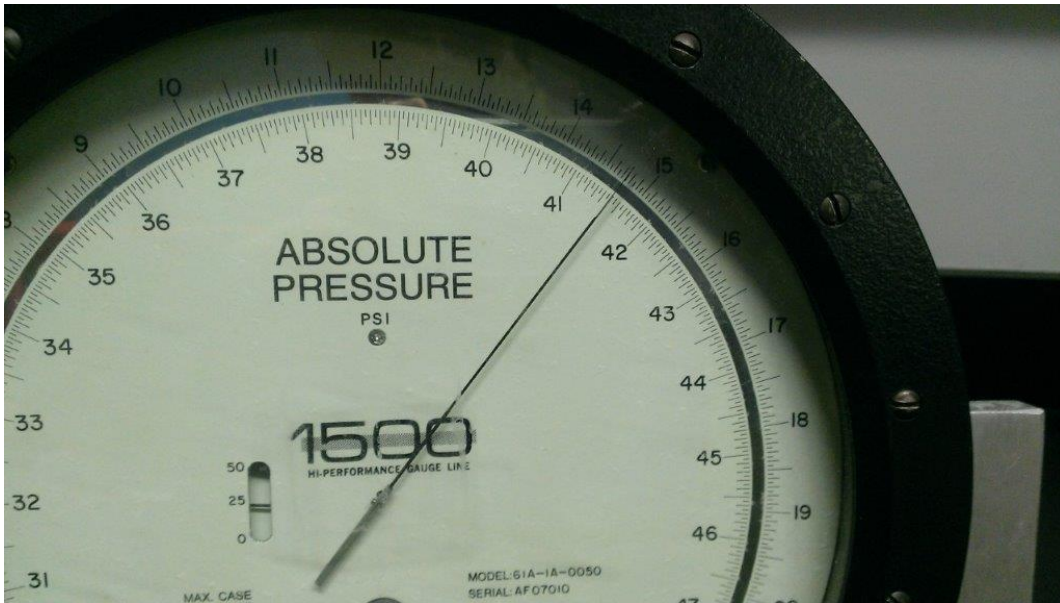


Figure 23: Barometer used for mass flow calibration experiment.

From the ideal gas law an equation to solve for the volume at STP (V_{STP}) can be derived.

$$\frac{PV}{T} = \text{constant}$$

$$V_{STP} = \frac{(P_R - P_{wv}) T_{STP}}{P_{STP} T_R} V_R$$

V_{STP} can be found using this derived equation, where P is pressure, V is volume, and T is temperature, and the subscript R is for room, wv is for water vapor, and STP is for STP. Then with this volume the volumetric flow rate in standard cubic centimeters (SCCM) can be calculated using the equation for volumetric flow rate from the beginning of this section.

In order to plot this data the average flow rate was found, however to ensure this average is accurate any outliers had to be removed. To determine any outliers the flow rate is subtracted by the average and then divided by the standard deviation and if this number is greater than two the flow rate is an outlier and is discarded.

$$\text{Outlier if } \frac{Q - Q_{avg}}{\sigma} > 2$$

Table 1 shows the average of the flow rate with the outliers excluded and its respective voltage. These values were then used to create the graph in Figure 24. The table of all the data recorded during the experiment is in Appendix 7.2. With this data the MATLAB program being used to control the mass flow system can be calibrated to allow for accurate measurements during experiments.

Voltage Read (V)	AVG Q w/o Outliers (SCCM)
0.48836	1.35515
1.48697	3.78431
2.48517	6.35103
3.48290	8.94405
4.47804	11.61459
4.97504	13.03517

Table 1: STP volumetric flow rate at set voltages.

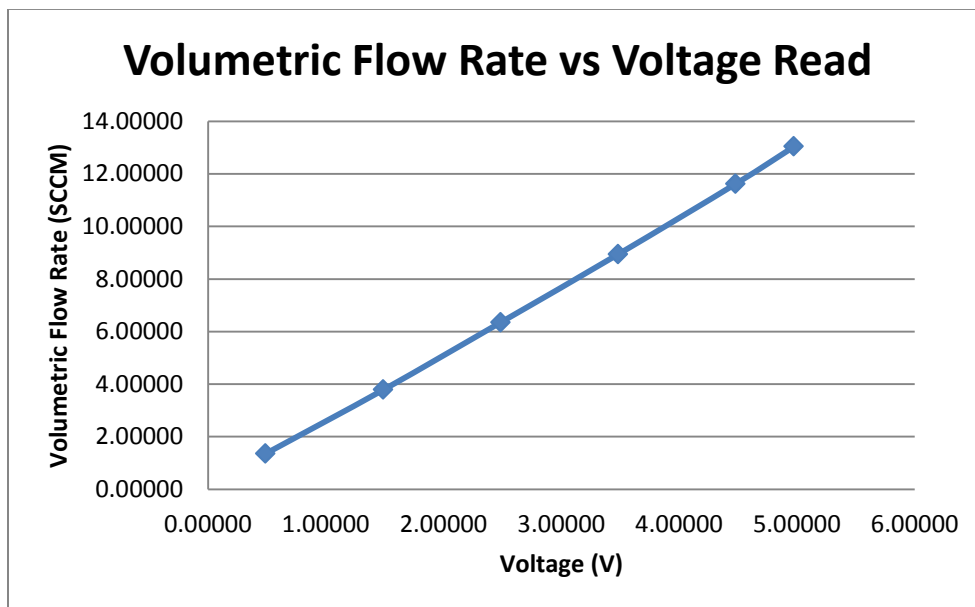


Figure 24: Graph of volumetric flow rate vs. voltage for mass flow calibration.

5. Summary and Recommendations

In this chapter we provide conclusions and recommendations for future work.

5.1 Summary and Conclusions

The main goal of this project was to design and fabricate a mounting assembly to be used within the Small Vacuum Facility-2 (SFV-2). The fabricated mounting assembly allows the attachment of plasma diagnostics to the positioning system. After several design iterations a finalized design of the necessary mount was concluded. The mount was designed in SolidWorks and machined in the Higgins Labs machine shop. A primary addition to the finalized mount was the bracketed rail system which allows for plasma probes of multiple lengths to be used in experiments.

Another goal of this MQP was to complete vibrational analysis of the SFV-2 using accelerometers. The data gathered from that experiment was then used in SolidWorks to estimate that the vibrations the chamber undergoes and position uncertainty of the probes attached to the mount.

The final goal of this MQP was to calibrate the mass flow system in SFV-2. This was done using an experiment involving a Bubble-O-Meter. With the calibrated mass flow system results from future experiments will be accurate and thus lead to valid conclusions.

Overall, this MQP achieved all major goals and an immense amount of knowledge was gained throughout the process. It was an insightful experience leaving all of us with extremely valuable understanding of these probes and the future experiments to be done.

5.2 Recommendations

In order to achieve the greatest accuracy during placement, future project groups should remove the mount at the circular base. By attaching and adjusting the probe outside the apparatus future project groups can be assured of greater accuracy with the placement of their probes. A two person team will also minimize the probability of unwanted adjustment when attaching the probe to the mount; one person to hold the mount at the desired location and the second person to screw down the pieces.

While we were able to determine that vibrations do permeate through the bell jar of the SFV-2 the full effect of the vibrations remains unknown due to the limitations of the equipment that was used. A future project group should acquire more sensitive equipment that do not have the data noise issues that our group had encountered and rerun the tests to determine the full extent and effect of the vibrations. In addition, the future project group should attempt to find an accelerometer that can measure in all three dimensions at once in order to evaluate the complete effect of the vibrations in 3-D space.

6. References

- Felder, R. M. & Rousseau R. W., "Elementary Principles of Chemical Processes," John Wiley & Sons, Inc. 3rd edition, Appendix B, p. 640-641, Table B.4, United States, 2005
- Gatsonis, N. A., and Yin, X., "Hybrid (particle-fluid) modeling of pulsed plasma thruster plumes" *Journal of Propulsion and Power*, 17, 5, pp. 945-958, Sept.-Oct. 2001.
- Gatsonis, N.A, Byrne. L., Zwahlen, J., Pencil, E., Kamhawi, H., "Current Mode Triple and Quadruple Langmuir Probe Methods with Applications to Flowing Pulsed Plasmas," *IEEE Transactions on Plasma Science*, 32, 5, pp. 2118-2129, October 2004.
- Goebel, D.M. & Katz, I., "Fundamentals of Electric Propulsion: Ion and Hall Thrusters" Jet Propulsion Laboratory California Institute of Technology, Pasadena, CA, March, 2008.
- Ketsdever, A.D., Wadsworth, D.C., & Muntz, E.P., "Predicted Performance and Systems Analysis of the Free Molecule Micro-resistojet," *Micropropulsion for Small Spacecraft, Progress in Astronautics and Aeronautics*, Vol. 187, American Institute of Aeronautics and Astronautics, Inc., 2000.
- MQP NAG-0902, Argueta, Dimitri Bakklas, Elias Karam, Smanatha Millar, David Wiig, , "Design of a Small Vacuum Facility for Microflow Experiments," WPI, Worcester, MA, April 2010.
- MQP NAG-1101, Andrew Baker, Andrew Bingham, Christopher Boucher, "Design of Setups for Plasma Propulsion Plume Experiments," WPI, Worcester, MA, March 2012.
- Partridge, J. & Gatsonis, N.A., "Preliminary Design and Analysis of a Directional Micro-Retarding Potential Analyzer for High-Density Plumes," AIAA-2003-5172, 39th AIAA/ASME/SAE/ASEE Joint Propulsion Conference & Exhibit, July 20-23, 2003, Huntsville, AL.
- Partridge, J. & Gatsonis, N.A., "Validation of a Directional Micro-Retarding Potential Analyzer for High-Density Plumes," AIAA-2005-3533, 41st AIAA/ASME/SAE/ASEE Joint Propulsion Conference & Exhibit, Tucson, AZ. July 10-13, 2005.
- Partridge, James, "Development and Implementation of Diagnostics for Unsteady Small-Scale Plasma Plumes." Ph. D. thesis, Department of Mechanical Engineering, WPI, Worcester, MA, September 2008.
- Simon, D.H., Land III, H. B., & Emhoff, J., "Experimental Evaluation of a Micro Pulsed Plasma Thruster Concept," AIAA-2006-4330, 42nd AIAA/ASME/SAE/ASEE Joint Propulsion Conference & Exhibit, July 9-12, 2006, Sacramento, CA.

7. Appendix

7.1 List of Laboratory Materials

Translation Motion Control

- Name: Microstepper Module Drive Model: SDM-20620 Serial: AZ-7901
 - o Galil Motion Control
- Name: Multi-Axis Motion Control Card Model: DMC-2123 Serial: AH-16434
 - o Galil Motion Control
- Name: Rotary Stage Serial: 06050211
 - o PiMicos
- Name: Linear Stage Serial: 06050210
 - o PiMicos

Ion Source

- Name: 3cm Kaufman Ion Source Power Supply ID2500 Model: 2001-002-A Serial: 8385
 - o Company Name: Pi Scientific

Vacuum System

- Name: Diffusion Pump Serial: LD0811L097 Model: 85826-311
 - o Varian
- Name: Roughing/Mechanical Pump Serial: 248125 Model: DS602
 - o LeRoy Somer 805419-2008
 - o Varian
- Name: High Vacuum Valve Serial: 102809-02 Model: LPWA6ASAN11SBEP
 - o Vacuum Research
- Name: Vent Valve Serial: 10-88427 Model: KIV-150-P
 - o MDC
- Name: Roughing Valve Serial: 10-88432 Model: KIV-150-P
 - o MDC
 - o Manual same as Vent Valve
- Name: Foreline Valve Serial: 10-88419 Model: KAV-150-B
 - o MDC

Pressure System

- Name: Oerlikon Leybold Vacuum Gage Controller (Chamber Pressure) Serial : 235004 F Number:332/2007 Model: Center Two
 - o Leybold Vacuum
 - o Printed Manual Found
- Name: Vacuum Gage Sensor (Chamber Pressure) Serial: 12090 Model: ITR090
 - o Leybold Vacuum
- Name: Foreline Pressure Sensor (Thermocouple Vacuum Gage) Serial:**** Model: 801w

- LDSVacuum.com
- Name: Vacuum Interlock Serial:***** Model:*****

Mechanical System

- Name: Water Pump Serial: D10J160066 Model: 5KH32GNB811AX
 - Marathon Electric
- Name: Hoist Serial: LPH500 Model: 615700
- Name: Wilkerson Regulator Serial: ***** Model: B28-04-FL00 28A
- Name: Gems Flow Switch Serial: ***** Model: FS-4
- Name: Water Valves X2 Category Number: WPSC8238T402

Mass Flow System

- Name: Canister of High Purity Argon Serial: 323 Model:
 - AIMTEK Inc.
- Name: Regulator Serial: 55850-474 Model: CGA E-4
 - VWR
- Name: Mass Flow Controller Serial: 021802153 Model: 1479A01311CR18M
 - MKS
 - MKS Type 1479A Mass Flo Controller
 - MKS Type 1179A and 2179A Mass Flo Controller and Type 179A Mass Flo meter
- Name: Mass Flow Power Supply Serial:***** Model: 246
 - MKS

Mass Flow Valves

- Name: DI/DS Series Diaphragm Valve
 - Swagelok

Data Acquisition and Control

- Name: Computer (KINOS) Serial: ***** Model: Dimension 9100
 - Name: Data Acquisition Card (inside computer)
 - Dell
- Name: Connector Block Serial: 15ECBA7 or 193184B-01L Model: SCC-68
 - National Instruments
- Name: LeCroy Oscilloscope Serial: LCRY0310M22369 Model: Wavesurfer 44Xs
 - LeCroy
- Name: Master Power Unit (Rename) Serial: Model:
 - Chas (insert Email here)

Feedthroughs

- 9-Pin D-Sub Connector
- Dual ¼" Swagelok VCR
- 8-Pin Octal Feedthrough
- 15-Pin D-Sub Connector
- Dual BNC Connector X6

- Dual MHV Connector X2

Power Supplies

- Name: BK Precision Power Supply Serial: 16720022606014162 Model: 1672
 - o BK Precision
- Name: BK Precision Power Supply Serial: N961500593 Model: 1671a
 - o BK Precision
- Name: BK Precision Power Supply Serial: A18500841 Model: 1620a
 - o BK Precision

Other

- Pressure Switches

7.2 Data from Mass Flow System Calibration Experiment

Trial #	Voltage Sending (V)	Voltage Receiving (V)	Avg VR (V)	Pressure (Psi)
1	0.5	0.4898		14.75
2	0.5	0.4875		14.75
3	0.5	0.4884		14.75
4	0.5	0.4881		14.75
5	0.5	0.4882		14.75
6	0.5	0.4882		14.75
7	0.5	0.4883	0.488357143	14.75
1	1.5	1.4873		14.75
2	1.5	1.4871		14.75
3	1.5	1.4866		14.75
4	1.5	1.4869		14.75
5	1.5	1.4871		14.75
6	1.5	1.4869		14.75
7	1.5	1.4869	1.486971429	14.75
1	2.5	2.4852		14.75
2	2.5	2.485		14.75
3	2.5	2.4851		14.75
4	2.5	2.4851		14.75
5	2.5	2.4854		14.75
6	2.5	2.4851		14.75
7	2.5	2.4853	2.485171429	14.75
1	3.5	3.4827		14.75
2	3.5	3.4832		14.75
3	3.5	3.483		14.75
4	3.5	3.4827		14.75

5	3.5	3.4829		14.75
6	3.5	3.483		14.75
7	3.5	3.4828	3.4829	14.75
1	4.5	4.478		14.75
2	4.5	4.478		14.75
3	4.5	4.4787		14.75
4	4.5	4.4781		14.75
5	4.5	4.478		14.75
6	4.5	4.4776		14.75
7	4.5	4.4779	4.478042857	14.75
1	5	4.9751		14.75
2	5	4.9754		14.75
3	5	4.9753		14.75
4	5	4.9748		14.75
5	5	4.975		14.75
6	5	4.9747		14.75
7	5	4.975	4.975042857	14.75

Pressure (Pa)	Temp (C)	Water Vapor Pressure (Psi)	Time (s)	Volume (ml or cm ³)
101697.5625	23.5	2894.81436	42.19	1
101697.5625	23.8	2947.606856	40.72	1
101697.5625	23.5	2894.81436	40.44	1
101697.5625	23.8	2947.606856	40.25	1
101697.5625	24	2983.266259	39.84	1
101697.5625	23.7	2929.916886	40.00	1
101697.5625	23.7	2929.916886	40.12	1
101697.5625	23.6	2912.319524	142.63	10
101697.5625	23.5	2894.81436	144.28	10
101697.5625	23.1	2825.707577	144.53	10
101697.5625	23.3	2860.079004	144.60	10
101697.5625	23.7	2929.916886	143.78	10
101697.5625	23.7	2929.916886	144.06	10
101697.5625	23.5	2894.81436	144.31	10
101697.5625	23.6	2912.319524	86.03	10
101697.5625	23	2808.657331	86.09	10
101697.5625	23.1	2825.707577	86.22	10
101697.5625	23.2	2842.848001	86.02	10
101697.5625	22.9	2791.696863	86.00	10
101697.5625	22.9	2791.696863	86.13	10

101697.5625	23	2808.657331	86.35	10
101697.5625	22.9	2791.696863	61.19	10
101697.5625	23	2808.657331	61.10	10
101697.5625	22.9	2791.696863	61.25	10
101697.5625	23	2808.657331	61.06	10
101697.5625	23.4	2877.400989	61.21	10
101697.5625	23.3	2860.079004	61.19	10
101697.5625	23	2808.657331	61.13	10
101697.5625	23	2808.657331	47.13	10
101697.5625	23.1	2825.707577	47.28	10
101697.5625	23.2	2842.848001	47.12	10
101697.5625	23.2	2842.848001	47.03	10
101697.5625	23.2	2842.848001	47.03	10
101697.5625	23.2	2842.848001	47.03	10
101697.5625	23.3	2860.079004	47.09	10
101697.5625	23.3	2860.079004	41.94	10
101697.5625	23.4	2877.400989	42.03	10
101697.5625	23.3	2860.079004	41.94	10
101697.5625	23.4	2877.400989	41.91	10
101697.5625	23.4	2877.400989	41.87	10
101697.5625	23.5	2894.81436	41.87	10
101697.5625	23.6	2912.319524	41.82	10

STP Volume (cm ³)	Mass Gage Readout	STP Q(SCCM)	AVG STP Q(SCCM)
0.909718389	140	1.293745043	
0.908313271	140	1.338379083	
0.909718389	140	1.349730548	
0.908313271	140	1.354007361	
0.907373834	140	1.366526859	
0.908782179	140	1.363173269	
0.908782179	140	1.359095981	1.346379735
9.092505507	420	3.824933958	
9.097183893	420	3.783137189	
9.11584478	420	3.784340184	
9.106524804	420	3.778640998	
9.087821791	420	3.792386336	
9.087821791	420	3.785015323	
9.097183893	420	3.782350728	3.790114959

9.092505507	700	6.341396378	
9.120496997	700	6.356485304	
9.11584478	700	6.34366373	
9.111187393	700	6.355164422	
9.125144075	700	6.366379587	
9.125144075	700	6.356770516	
9.120496997	700	6.337345916	6.351029408
9.125144075	979	8.947681721	
9.120496997	979	8.956298197	
9.125144075	979	8.938916645	
9.120496997	979	8.962165408	
9.101856981	979	8.921931365	
9.106524804	979	8.92942455	
9.120496997	979	8.951902827	8.944045816
9.120496997	1258	11.61107192	
9.11584478	1258	11.56833094	
9.111187393	1258	11.60168174	
9.111187393	1258	11.62388355	
9.111187393	1258	11.62388355	
9.111187393	1258	11.62388355	
9.106524804	1258	11.60313205	11.60798105
9.106524804	1397	13.02793248	
9.101856981	1397	12.99337185	
9.106524804	1397	13.02793248	
9.101856981	1397	13.03057549	
9.101856981	1397	13.0430241	
9.097183893	1397	13.03632753	
9.092505507	1397	13.04520159	13.02919507

Sqrd. Dif. From AVG	Standard Deviation	Outlier if >2	AVG Q w/o Outliers
0.002770411		2.273029569	
6.40104E-05		0.345508188	
1.12279E-05		0.144704894	
5.81807E-05		0.329399095	
0.000405907		0.870053701	
0.000282023		0.725228889	
0.000161703	0.023156184	0.549151178	1.355152183
0.001212363		2.364835159	
4.86893E-05		0.473915919	

3.3348E-05		0.392210923	
0.000131652		0.779288018	
5.15915E-06		0.154267278	
2.60063E-05		0.346356869	
6.02833E-05	0.014723647	0.527330708	3.784311793
9.27953E-05		0.999866789	
2.97668E-05		0.56629844	
5.42532E-05		0.764525449	
1.70983E-05		0.429196611	
0.000235628		1.593282247	
3.29603E-05		0.595902184	
0.000187238	0.009634313	1.420287245	6.351029408
1.32198E-05		0.268613288	
0.000150121		0.905181052	
2.63084E-05		0.378932774	
0.00032832		1.338638748	
0.000489049		1.633770848	
0.000213781		1.080189509	
6.17326E-05	0.013535834	0.580460044	8.944045816
9.55354E-06		0.166803317	
0.001572131		2.139769472	
3.96813E-05		0.339950208	
0.00025289		0.858199564	
0.00025289		0.858199564	
0.00025289		0.858199564	
2.35128E-05	0.018530083	0.26168233	11.6145894
1.59414E-06		0.079028571	
0.001283303		2.242257588	
1.59414E-06		0.079028571	
1.90556E-06		0.086403566	
0.000191242		0.865590161	
5.08719E-05		0.446436619	
0.000256208	0.015976408	1.001884385	13.03516561